On the Privacy Risks of Model Explanations

Reza Shokri, Martin Strobel, Yair Zick
School of Computing
National University of Singapore

Abstract

Privacy and transparency are two key elements of trustworthy machine learning. Model explanations can provide more insight into a model's decisions on input data. This, however, can impose a significant privacy risk to the model's training set. We analyze whether an adversary can exploit model explanations to infer sensitive information about the model's training set. We investigate this research problem primarily using *membership inference attacks*: inferring whether a data point belongs to the training set of a model given its explanations. We study this problem for three popular types of model explanations: backpropagation-based, perturbation-based and example-based attribution methods. We devise membership inference attacks based on these model explanations, and extensively test them on a variety of datasets. We show that both backpropagation- and example-based explanations can leak a significant amount of information about individual data points in the training set. More importantly, we design *reconstruction attacks* against example-based model explanations, and use them to recover significant parts of the training set. Finally, we discuss the resistance of perturbation-based attribution methods to existing attack models; interestingly, their resistance to such attacks is related to a crucial shortcoming of such model explanations uncovered by recent works.

1   Introduction

Black-box machine learning models are often used to make high-stakes decisions in sensitive domains. However, their inherent complexity makes it extremely difficult to understand the underlying *reasoning* for their decisions. This has resulted in a mounting pressure from the general public and government agencies; several proposals advocate for deploying (automated) *model explanations* [19]. Novel explanation methods have been proposed in recent years; Google, Microsoft and IBM now offer model explanation toolkits as part of their ML suites.[1]

Model explanations offer users additional insights, or information about the model, with respect to the particular decisions it makes on their data records. Releasing additional information is, however, a risky prospect from a privacy perspective. The explanations, as functions of the model trained on a private dataset, might inadvertently leak information about the training set, beyond what is necessary to provide useful explanations. Despite this potential risk, there has been little effort to analyze and address any data privacy concerns that might arise due to the release of model explanations. This is where our work comes in. We initiate this line of research by asking the following question: **can an adversary leverage model explanations to infer private information about the training data?**

Our Contributions   Our work is the first to analyze the *data* privacy risks that arise from releasing model explanations, which can result in a tradeoff between transparency and privacy. We provide a comprehensive analysis of information leakage through feature-based and example-based

---

[1]See http://aix360.mybluemix.net/, https://aka.ms/AzureMLModelInterpretability and https://cloud.google.com/explainable-ai

model explanations. We analyze *backpropagation-based* model explanations, with an emphasis on gradient-based methods [38], *perturbation-based* methods [42]; we also analyze *example-based* model explanations, with an emphasis on a method that reports influential data points [22]. For *backpropagation-based explanations*, we identify potential causes for the leakage, and design adversarial inference algorithms that effectively identify members of the training set; these are also known as *membership inference attacks* [35]. For *example-based explanations*, our algorithms can reconstruct a large fraction of the training data (referred to as *dataset reconstruction attacks* [16]).

We analyze what information the gradient-based explanations can leak about the training data, and compare our approach to the strongest type of membership inference attack, that have access to the model's loss on data points. We show that the *variance* of backpropagation-based explanations can help identifying the training set members. This may be due, in part, to how backpropagation-based training algorithms behave upon convergence. However, experiments on synthetic data indicate that the relation between variance and training data membership is greatly affected by data dimensionality. Perturbation-based explanations, such as SmoothGrad [42], are seemingly resistant to this type of attack. We attribute this to the fact that they rely on out-of-distribution samples to generate explanations. This, however, can have negative effects on explanation fidelity.

Example-based model explanations provide influential training data points for the decision on a particular point of interest. This presents an obvious leak of training data. In particular, membership inference attacks are much simpler: we show that training points are frequently used to explain their own predictions. We focus on a more ambitious objective of reconstructing the entire training dataset. Randomly querying the model, however, does not recover many points. This is because a few certain training data records — especially mislabeled training points at the border of multiple classes — have greater influence over most of the input space. Thus, after a few queries, the set of reconstructed data points converges. We design an algorithm that identifies and constructs regions of the input space where previously recovered points will not be influential. This avoids rediscovering previously revealed points, and improves the attack's coverage. We prove a worst-case upper bound on the number of recoverable points and show that our algorithm is optimal in the sense that for worst case scenarios it recovers all possible points.

Through empirical evaluations of example-based model explanations on various datasets, we show that **an attacker can reconstruct (almost) the entire dataset for high dimensional data**. For datasets with low dimensionality, we demonstrate our heuristic's adaptability by using the previously recovered points. In the data we study the graph structure, induced by the influence function over the training set, tends to have a small number of large strongly connected components, and the attacker is likely to recover at least all points in one of them.

We further study the effectiveness of membership inference attacks based on additional backpropagation-based explanations (including Integrated Gradients and LRP). These attacks achieve comparable, albeit weaker, results than attacks against gradient-based explanations. We also present the results of studying the influence of dataset size on the success of membership inference for example-based explanations. Finally, as unusual points tend to have a larger influence on the training process, we show that **training data of minorities can have a high risk of being revealed**. These results (as well as others) are relegated to the supplementary material.

2 Background

We are given a labeled *dataset* $\mathcal{X} \subseteq \mathbb{R}^n$, with n features and k labels. The labeled dataset is used to train a *model* c, which maps each *datapoint* $\vec{x}$ in $\mathbb{R}^n$ to a distribution over k *labels*, indicating its belief that any given label fits $\vec{x}$. Black-box models often reveal the label deemed *likeliest* to fit the datapoint. The model is defined by a set of *parameters* θ taken from a *parameter space* Θ. We denote the model as a function of its parameters as c_θ. A model is trained to empirically minimize a *loss function* over the training data. The loss function $L : \mathcal{X} \times \Theta \to \mathbb{R}$ takes as input the model parameters θ and a point $\vec{x}$, and outputs a real-valued loss $L(\vec{x}, \theta) \in \mathbb{R}$. The objective of a machine-learning algorithm is to identify an *empirical loss minimizer* over the parameter space Θ:

$$\hat{\theta} \in \mathrm{argmin}_{\theta \in \Theta} \frac{1}{|\mathcal{X}|} \sum_{\vec{x} \in \mathcal{X}} L(\vec{x}, \theta) \tag{1}$$

2.1 Model Explanations

As their name implies, model explanations explain model decisions on a given *point of interest* (POI) $\vec{y} \in \mathbb{R}^n$. An explanation ϕ takes as input the dataset $\mathcal{X}$, labels over $\mathcal{X}$ — given by either the true labels $\ell : \mathcal{X} \to [k]$ or by a trained model c — and a *point of interest* $\vec{y} \in \mathbb{R}^n$. In addition, explanation methods sometimes assume access to additional information, such as active access to model queries (e.g. [2, 13, 32]), a prior over the data distribution [6], or knowledge of the model class (e.g. that the model is a neural network [5, 37, 47], or that we know the source code [14]). The output of an explanation function $\phi(\mathcal{X}, c, \vec{y}, \cdot)$ can be quite diverse (here the $\cdot$ operator stands for potential additional inputs); in this work we focus on two explanation paradigms: *example-based* explanations [22] , and *feature-based* attribution methods. More formally, example-based explanations output a set of points $\phi(\mathcal{X}, c, \vec{y}, \cdot) \subseteq \mathcal{X}$, whereas feature-based methods output a vector in $\mathbb{R}^n$. For feature-based methods, we focus on backpropagation-based methods [38] and perturbation-based methods[13, 32, 42]. In what follows we often refer to the explanation of the POI $\vec{y}$ as $\phi(\vec{y})$, omitting its other inputs when they are clear from context.

2.1.1 Feature-Based Explanations

A feature-based explanation $\phi(\vec{y})$ is a vector in $\mathbb{R}^n$, where $\phi_i(\vec{y})$ is the degree to which the i-th feature influences the label assigned to $\vec{y}$. Generally speaking, high values of $\phi_i(\vec{y})$ imply a greater degree of effect; negative values imply an effect for *other labels*; a $\phi_i(\vec{y})$ close to 0 normally implies that feature i was largely irrelevant. Ancona et al. [4] provide a recent overview of feature-based explanations (also called attribution methods). Many feature-based explanation techniques are implemented in the INNVESTIGATE library[2] [3] which we use in our experiments.

Backpropagation-Based Explanations Backpropagation-based methods rely on a small number of backpropagations through a model to attribute influence from the prediction back to each feature. The canonical example of this type of explanation is the gradient with respect to the input features [38], we focus our attack on this explanation. Other backpropagation-based explanations have been proposed [6, 21, 36, 41, 42, 47]. We analyze some of them in Appendix B.

Perturbation-Based Explanations Perturbation-based methods query the to-be-explained model on many perturbed inputs. They either treat the model as a black-box [12, 32], need predictions for counterfactuals [12], or 'smooth' the explanation [42]. They can be seen as local linear approximations of a model. We focus on SmoothGrad [42], which generates multiple samples by adding Gaussian noise to the input and releases the averaged gradient of these samples. Formally for some $k \in \mathbb{N}$, $\phi_{SMOOTH}(\vec{x}) = \frac{1}{k} \sum_k \nabla c(\vec{x} + \mathcal{N}(0, \sigma))$, where $\mathcal{N}$ is the normal distribution and σ is a hyperparameter.

2.1.2 Example-Based Explanations

For example-based model explanations, we focus on the approach proposed by Koh and Liang [22]. It aims at identifying influential *datapoints*; that is, given a point of interest $\vec{y}$, find a subset of points from the training data $\phi(\vec{y}) \subseteq \mathcal{X}$ that explains the label $c_{\hat{\theta}}(\vec{y})$, where $\hat{\theta}$ is a parameterization induced by a training algorithm A. It selects a training point $\vec{x}_{\text{train}}$ by measuring the importance of $\vec{x}_{\text{train}}$ for determining the prediction for $\vec{y}$.

To estimate the effect of $\vec{x}_{\text{train}}$ on $\vec{y}$, the explanation measures the difference in the loss function over $\vec{y}$ when the model is trained with and without $\vec{x}_{\text{train}}$. Let $\theta_{\vec{x}_{\text{train}}} \triangleq A(\mathcal{X} \backslash \{\vec{x}_{\text{train}}\})$, in words, $\theta_{\vec{x}_{\text{train}}}$ is induced by training algorithm A given the dataset excluding $\vec{x}_{\text{train}}$. The influence of $\vec{x}_{\text{train}}$ on $\vec{y}$ is then

$$I_{\vec{y}}(\vec{x}_{\text{train}}) \triangleq L(\vec{y}, \theta_{\vec{x}_{\text{train}}}) - L(\vec{y}, \hat{\theta}). \tag{2}$$

The Koh and Liang explanation releases the k points with the highest absolute influence value according to Equation (2). Additionally, it might release the influence of these k points (the values of $I_{\vec{y}}(\vec{z})$ as per Equation (2)), which allows users to gauge their relative importance.

2.2 Membership Inference Attacks

Models tend to have lower loss on members of the training set. Several works have exploited this fact to define simple loss-based attacks [26, 34, 48]. The idea is to define a threshold τ: an input $\vec{x}$ with a
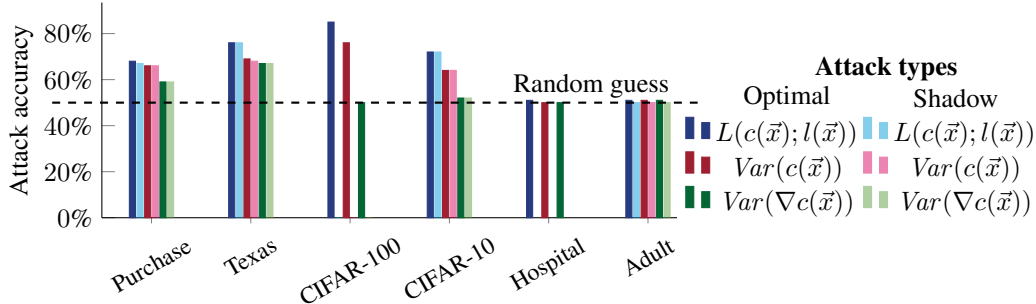
---

[2]https://github.com/albermax/innvestigate

Figure 1: Results for the threshold-based attacks using different attack information sources. The OPTIMAL attack uses the optimal threshold; the SHADOW trains a shadow model on data from the same distribution, and uses an optimal threshold for the shadow model. Using three such models results in nearly optimal attack accuracy. We omit SMOOTHGRAD-based results due to low accuracy.

loss $L(\vec{x}, \theta)$ lower than τ is considered a member; an input with a loss higher is considered a non-member. Sablayrolles et al. [34] show that this attack is optimal given an optimal threshold τ_{opt}, under some assumptions. However, this attack is infeasible in cases where the attacker doesn't have access to the true labels, or the model's loss function. Hence, we propose to generalize threshold-based attacks to different sources of information. Explicitly, we consider (i) a threshold on the prediction variance and (ii) a threshold on the explanation variance. Access to both these types of information is easier as they are provided by the target model. A target model might *only release the predicted label and an explanation*, making only explanation-based attacks feasible.

Our explanation-based threshold attacks work in a similar manner to other threshold-based attack models: we measure the variance of the model explanation $\phi(\vec{y})$ at $\vec{y}$; if it is below a certain threshold τ it is considered a member; otherwise it is considered a non-member. The crucial part is obtaining the threshold τ. We consider two scenarios:

1. **Optimal threshold** For a given set of members and non-members there is a threshold τ_{opt} that achieves the highest possible prediction accuracy for the attacker. This threshold can easily be obtained when datapoint membership is known. This approach should not be seen as an actual attack. Rather, the performance of τ_{opt} provides an upper bound on what an attacker with otherwise unlimited resources can achieve using a threshold attack.

2. **Reference/Shadow model(s)** This assumes that the attacker has access to some labeled data from the target distribution. The attacker trains s models on that data and calculates the threshold for these reference (or shadow) model. In line with Kerckhoffs's principle [31] we assume that the attacker has access to the training hyper parameters and model architecture. This attack becomes increasingly resource intensive as s grows. For our experiments we choose $s \in \{1, 3\}$.

3 Privacy Analysis of Feature-Based Explanations

We use the Purchase and Texas datasets in [29]; we also test CIFAR-10 and CIFAR-100 [34], the Adult dataset [15] as well as the Hospital dataset [45]. The last two datasets are the only binary classification tasks considered. Where possible, we use the same training parameters and target architectures as the original papers (see Appendix A for details). We study four types of information the attacker could use: loss, prediction variance, gradient variance and the SmoothGrad variance.

3.1 Evaluation

Explanation-based attacks Gradient-based attacks (as well as other backpropagation-based methods, as shown in Appendix B) on the Purchase and Texas datasets were successful. This is a *clear proof of concept* that model explanations can be exploited for membership inference. However, the attacks were ineffective for the image datasets; gradient variance fluctuates wildly between individual images, making it difficult to infer membership. Attacks using SmoothGrad perform poorly; this phenomenon holds for other perturbation-based methods, and is discussed in Section 3.3. When

loss-based attacks are successful, prediction-based attacks are nearly as successful. This demonstrates that it is not essential to assume that the attacker knows the true label of the point of interest, which opens up attack scenarios in many novel domains. The dataset type (and model architecture) greatly influences attack success. For both binary datasets (Texas and Purchase), all sources of information pose a threat. On the other hand, for the very low dimensional Hospital and Adult datasets, none of the attacks outperform random guessing. This may be due to the fact that the target model is not overfitted to the data, which generally limits its vulnerability to adversarial attacks [48]. Shadow model based attacks compare well to the optimal attack, with attacks based on three shadow model performing nearly at an optimal level; this is in line with results for loss-based attacks [34].

3.2 Additional Analysis

To study the influence of *training set dimensionality* on attacks, we generate datasets of increasing dimension, and train a network with a fixed architecture. Attacks are inaccurate for very high and low dimensional datasets, and perform well for mid-range dimensional datasets. Within the mid-range of data dimension, models overfit most to the training data; see the complete analysis (with different architectures and data) in Appendix C.

In the attacks above we used only the variance of the explanations. Intuitively, when the model is certain about a prediction, because it is for a training point, it is unlikely to change the prediction with small local perturbation i.e. the influence (and attribution) of each feature is low. Hence, it has a smaller explanation variance. For points closer to the decision boundary, changing a feature effects the prediction stronger i.e. the variance of the explanation should be higher. In fact, the loss minimization during training tries to "push" points away from the decision boundary. Especially, models using `tanh`, sigmoid or softmax activations have steep gradients in the areas where the output changes. Training points generally don't fall into these areas.[3] Hence, explanation variance is a sufficient parameter for deploying a successful attack. To further validate this claim, we conduct an alternative attack using the entire explanation vector as input. This is based on the method of Shokri et al. [35], who formulate membership inference as a learning problem for the attacker and train a neural network to predict membership. This formulation allows for very flexible information sources. Our results indicate that attacks using the explanation variance are only slightly weaker than attacks using the entire explanation vector, even when we assume that the attacker has access to parts of the original training method; see Appendix D.

Yeom et al. [48] show that *overfitting significantly influences the accuracy of membership inference attacks*. To test the effect of overfitting, we vary the number of iterations of training achieving different accuracies. In line with previous findings for loss-based attacks, our threshold-based attacks using explanations and predictions work better on overfitted models; see Appendix E.

3.3 Membership Inference Attacks against Perturbation-Based Model Explanations

Neither the threshold-based attacks described in Section 2.2 nor the learning-based attacks in Appendix D outperform random guessing when given access to perturbation-based methods.[4] While it is entirely possible that perturbation-based methods are vulnerable to membership inference, we conjecture that this is not the case. This is due to an interesting connection between perturbation-based model explanations and the *data-manifold hypothesis* [17]. The data-manifold hypothesis states that "data tend to lie near a low dimensional manifold" [17, p. 984]. Many works support this hypothesis [8, 9, 28], and use it to explain the pervasiveness of adversarial examples [18]. To the best of our knowledge, little is known on how models generally perform outside of the data manifold. In fact, it is not even clear how one would measure performance of a model on points outside of the training data distribution: they do not have any natural labels. Research on creating more robust models aims at decreasing model sensitivity to small perturbations, including those yielding points outside of the manifold. However, robustness results in vulnerability to membership inference [43]. Perturbation-based explanation methods have been criticized for not following the distribution of the training data and violating the manifold hypothesis [25, 46]. Slack et al. [40] demonstrate how a

---

[3]The high variance described here results from higher absolute values, in fact instead of the variance an attacker could use the 1-norm. In our experiments, there was no difference between using 1-norm and using variance and we decided to use variance to be more consistent with the prediction threshold.

[4]We test SmoothGrad [42], as well as LIME [32]; however the latter takes relatively long to compute and we run smaller experiments (see Appendix F).

malicious actor can differentiate normal queries to a model from queries generated by LIME and QII, and so make a biased model appear fair during an audit. Indeed, the resilience of perturbation-based explanations to membership inference attacks may very well stem from the fact that query points that the model is not trained over, and for which model behavior is completely unspecified. One can argue that the fact that these explanations do not convey membership information is a major *flaw* of this type of explanations. Given that the results in the previous section indicate that for many training points the model heavily overfits — to the extent that it effectively "memorizes" labels — an explanation should reflect that.

4 Dataset Reconstruction Attacks via Example-Based Model Explanations

In this section we analyze how many training points an attacker can recover with access to example-based explanations. We focus on logistic regression models, for which example-based explanations were originally used [22]. The results can be generalized to neural networks by focusing only on the last layer, we demonstrate this by considering a binary image classification dataset used in [22]; we call this dataset Dog/Fish. We also focus only on binary classification tasks. While technically the approaches discussed in previous sections could be applied to this setting as well, example-based explanations allow for stronger attacks. Specifically, they explicitly reveal training points, and so offer the attacker certainty about a points' training set membership (i.e. no false positives). Formally, we say a point $\vec{y}$ *reveals* point $\vec{x}$ if for all $z \in \mathcal{X}$, $|I_{\vec{y}}(\vec{x})| \geq |I_{\vec{y}}(\vec{z})|$. In other words, $\vec{x}$ will be offered if one requests a example-based explanation for $\vec{y}$. Similarly, $\vec{y}$ *k-reveals* point $\vec{x}$ if there is a subset $S \subseteq \mathcal{X}, |S| = k - 1$ such that $\forall z \in \mathcal{X} \backslash S\colon |I_{\vec{y}}(\vec{x})| \geq |I_{\vec{y}}(\vec{z})|$. Hence, $\vec{x}$ will be one of the points used to explain the prediction of $\vec{y}$ if one releases the top k most influential points. A point $\vec{x} \in \mathcal{X}$ that (k-)reveals itself, is called *(k-)self-revealing*.

Revealing membership for example-based explanations While for feature-based explanations the attacker needs to rely on indirect information leakage to infer membership, for example-based explanations, the attacker's task is relatively simple. Intuitively, a training point should be influential for its own prediction, so an example-based explanation of a training set member is likely to contain the queried point, revealing membership. We test this hypothesis via experiments, i.e. for every point $\vec{x} \in \mathcal{X}$ in the training set we obtain the $k \in \{1, 5, 10\}$ most influential points for the prediction $f_\theta(\vec{x})$ and see if $\vec{x}$ is one of them.

We conduct the experiments on three different binary classification tasks. Details are provided in Appendix G. The revelation rate ranges from 10% (for Adult and $k = 1$) to 75% (for Hospital and $k = 10$). For the standard setting where the top 5 most influential points are revealed (i.e. $k = 5$), on average at least a quarter of each dataset is revealed. We also found indications that outliers and certain hard to generalize minorities are at a higher risk of being revealed.

Analysis For Dataset Reconstruction Let us now turn our attention to a stronger type of attack; rather than inferring the membership of specific datapoints, we try to recover the *training dataset*.

Lower and upper bounds It is relatively easy to construct examples in which only two points in the dataset can be revealed. In fact, there are specific instances in which only a single datapoint can be revealed, however these cases are neither particularly insightful nor do they reflect real-world settings. On the other hand, there exist datasets with an arbitrarily high number of features which can be fully recovered using (see Appendix H.2).

We construct a practical algorithm with which the attacker can iteratively reveal new points. Algorithm 1 (formally stated in Appendix H.1) consists of two main steps (1) Sample a point in the current subspace and (2) find a new subspace in which all already discovered points have zero influence, and continue sampling in this subspace.

Theorem 4.1 offers a lower bound on the number of points that Algorithm 1 discovers. The theorem holds under the mild assumption on the sampling procedure, namely that when sampling from a subspace R of dimension k, the probability of sampling a point within a given subspace Q of dimension $< k$ is 0. This assumption is fairly common, and holds for many distributions, e.g. uniform sampling procedures. We say that a set of vectors Q is d-wise linearly independent if every subset $D \subseteq Q$ of size d is linearly independent. For a dataset $\mathcal{X} \subset \mathbb{R}^n$ and a training algorithm A, we say that the model parameters $\theta = (\vec{w}, b)$ are induced by $\mathcal{X}$ and write $(\vec{w}, b) \triangleq A(\mathcal{X})$.

Theorem 4.1. *Given a training set $\mathcal{X} \subset \mathbb{R}^n$, let $\theta = (\vec{w}, b)$ be the parameters of a logistic regression model induced by $\mathcal{X}$. Let $d \in \mathbb{N}$ be the largest number such that the vectors in $W = \{\vec{w}_{\vec{x}} | \vec{x} \in \mathcal{X}, (\vec{w}_{\vec{x}}, b_{\vec{x}}) \triangleq A(\mathcal{X} \backslash \{\vec{x}\})\}$ are d-wise linearly independent, then if all vectors in W are linearly independent of $\vec{w}$, Algorithm 1 (with query access to model predictions and example-based explanations) reveals at least d points in $\mathcal{X}$ with probability 1.*

For the proof of Thoerem 4.1 see Appendix I. Algorithm 1 recovers large parts of the dataset for high-dimensional data. If $d \geq |\mathcal{X}|$, it can recover the entire dataset. For $d \ll |\mathcal{X}|$, only a small part of the dataset will be recovered. Algorithm 1 is optimal in the sense that there are datasets for which only the points discovered by the algorithm can be discovered (see Figure 13 (Left)). However, there are many situations where the algorithm falls short of discovering all possible points (see Figure 13 (Right)). Furthermore, the algorithm does not exploit the fact that in practical situations the k most influential points would be revealed, instead of just one. In fact, incorporating the information about the k-most influential points into Algorithm 1 yields negligible benefits. The following heuristic offers no theoretical guarantees, but works well even when $d \ll |\mathcal{X}|$, as we show next.

Querying Revealed Points   This heuristic is relatively simple: use previously revealed points to reveal new points. When querying a point the Koh and Liang measure returns k training points (and their influence) as explanations. The attacker can now use these revealed points in new queries, obtaining new points from these queries. This naturally defines an *influence graph* structure over the training set: Every point in the training set is a node v in a graph G, with k outgoing edges towards the k nodes outputted by the Koh and Liang measure. The influence graph structure governs the degree to which one can adaptively recover the training set. For example, if the graph contains only one strongly connected component, an attacker can traverse (and recover) the entire training set from a single starting point. The following metrics are particularly informative:

Number of strongly connected components (SCCs): a high number of SCCs implies that the training set is harder to recover: an adaptive algorithm can only extract one SCC at a time. It also implies that the underlying prediction task is fragmented: labels in one part of the dataset are independent from the rest.

Size of the SCCs: large SCCs help the attacker: they are more likely to be discovered, and recovering just some of them already results in recovery of significant portions of the training data.

Distribution of in-degrees: the greater a node's in-degree is, the likelier its recovery; for example, nodes with zero in-degree may be impossible for an attacker to recover. Generally speaking, a uniform distribution of in-degrees makes the graph easier to traverse.

Dataset	n	$|\mathcal{X}|$	# points recovered	% of $|\mathcal{X}|$
Dog/Fish	2048	1,800	1790	99.4
Adult	104	2,000	91.5	4.6
Hospital	127	2,000	81.1	4.0

Table 1: The number of points recovered using our attack based on subspace reduction. For small sized, high dimensional data, notably Dog/Fish, the attack can recover (almost) the entire dataset.
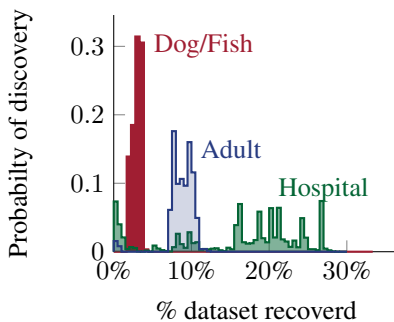
Figure 2: Distribution over the size of the revealed training data, starting from a random point in the influence graph. This is obtained by averaging over 10 initiations of the training set. Each time roughly the size of the largest SCC is recovered. For the Hospital dataset the size of the SCC varies the most, hence the multimodal distribution.

	Dog/Fish	Adult	Hospital
#SCC	1709	1742	1448
#SCC of size 1	1679	1701	1333
Largest SCC size	50	167	228
Max in-degree	1069	391	287
#node in-degree=0	1364	1568	727

Table 2: Some key characteristics of the influence graphs induced by the example-based explanations (for $k = 5$). This is averaged over 10 random initializations of the training set

Dataset Reconstruction for Example-Based Explanations   We evaluate our reconstruction algorithms on the same datasets as the membership inference for example-based explanations. In this section we describe the results for the two approaches described above. In Appendix J we compare them to some general baselines.

Attack based on subspace reduction Table 1 summarizes the results from our attack based on Algorithm 1. For Dog/Fish, we recover (nearly) the *entire* dataset. The number of recovered points for Adult and Hospital is small compared to the size of the dataset, but especially for Adult close to the dimensionality of the data, which is the upper bound for the algorithm. In our actual implementation, rather than constructing the subspaces and sampling points in them we recovered the entire weight vectors and sampled points by solving a least squares optimization problem with some additional constraints to increase numerical stability.

Adaptive heuristic attack Table 2 summarizes some key characteristics of the influence graphs for the training datasets (in this section we set $k = 5$, larger values of k lead to similar results). Remarkably, the influence graphs are fragmented, comprising of a large number of connected components, most of which have size 1. Each graph seems to have one larger SCC, which most of the smaller SCCs point to. This implies that an attacker starting at a random point in the graph is likely to recover only slightly more than the largest SCC. In fact, a significant amount of points (up to 75% for the Adult dataset) have in-degree 0: they cannot be recovered by this adaptive attack. Figure 2 illustrates the percentage of the dataset recovered when traversing the influence graph from a random starting point. For the Dog/Fish dataset, the largest SCC is revealed every time. For the Adult and Hospital datasets the largest SCC is not revealed for some points, resulting in limited success.

The order of queries does not affect the overall success of the attack, eventually every point reachable from the initial query will be revealed. However, minimizing the number of initial queries used is desirable.The number of queries required to traverse the discoverable part of the influence graph is stable under changes to the query schedule (e.g. BFS, DFS, random walk and several influence-based heuristics resulted in similar performance). In order to benchmark the performance of our attacker, who has no knowledge of the influence graph structure, we compare it to an omniscient attacker who knows the graph structure and is able to optimally recover the SCCs; this problem is known to be NP-complete (the best known constant factor approximation factor is 92) [11]. We thus compare our approach to a greedy omniscient attacker, which selects the node that is connected to the most unknown points. Compared to this baseline, our approaches require roughly twice as many queries.

5   Related Work, Conclusions and Future Work

In a recent paper, Milli et al. [27] show that gradient-based explanations can be used to reconstruct the underlying model; this serves as additional evidence of the vulnerability of transparency reports. There exists some work on the defense against privacy leakage in advanced machine learning models. Abadi et al. [1] and Papernot et al. [30] have designed frameworks for differentially private training of deep learning models. However, training *accurate* and privacy-preserving models is still a challenging research problem. In addition, the effect of these techniques (notably the randomness they induce) on model transparency is unknown.

Our results are just a first step towards a better understanding of transparency-based privacy attacks; several interesting open problems remain. For example-based explanations, it is unclear how one can offer safety guarantees. While low dimensional datasets are relatively robust against our subspace reduction attack, they are vulnerable to influence graph-based attacks. While our theoretical analysis is restricted to logistic regression, the attacks can be extended to more complicated models: the general principle of minimizing the influence of discovered points allows for a model-agnostic gradient-descent based attack. The influence graphs used in our analysis might be of separate interest: their characteristics highlight how a model "structures" the training set; their further study may lead to insights about the behavior of different model types, and provide an avenue for better example-based model explanations. Finally, designing safe transparency reports is an important research direction: one needs to release explanations that are both safe, and formally useful. For example, releasing no explanation (or random noise) is guaranteed to be safe, but is clearly not useful; example-based explanations are useful, but are not safe. Quantifying the quality/privacy trade-off in model explanations will help us understand the capacity to which one can explain model decisions, while maintaining data integrity.

Broader Impact

AI governance frameworks call for transparency and privacy for machine learning systems.[5] Our work investigates the potential negative impact of explaining machine learning models, in particular, it shows that offering model explanations may come at the cost of user privacy. The demand for automated model explanations led to the emergence of model explanation suites and startups. However, none of the currently offered model explanation technologies offer any provable privacy guarantees. This work has, to an extent, arisen from discussion with colleagues in industry and AI governance; both expressed a great deal of interest in the potential impact of our work on the ongoing debate over model explainability and its potential effects on user privacy.

One of the more immediate risks is that a real-world malicious entity uses our work as the stepping stone towards an attack on a deployed ML system. While our work is still preliminary, this is certainly a potential risk. Granted, our work is still at the proof-of-concept level, and several practical hurdles must be overcome in order to make it into a fully-fledged deployed model, but nevertheless the risk exists. In addition, to the best of our knowledge, model explanation toolkits have not been applied commercially on high-stakes data. Once such explanation systems are deployed on high-stakes data (e.g., for explaining patient health records or financial transactions), a formal exploration of their privacy risks (as is offered in this work) is necessary.

Another potential impact — which is, in the authors' opinion, more important — is that our work implies an *inevitable* conflict between explaining ML models — the celebrated "right to explanation" — and preserving user privacy. This tradeoff needs to be communicated beyond the ML research community, to legal scholars and policymakers. The explainability/privacy conflict disparately impacts minority groups: their data is either likelier to be revealed, else they will receive low quality explanations. We do not wish to make a moral stand in this work: explainability, privacy and fairness are all noble goals that we should aspire to achieve. Ultimately, it is our responsibility to explain the capabilities — and limitations — of technologies for maintaining a fair and transparent AI ecosystem to those who design policies that govern them, and to various stakeholders. Indeed, this research paper is part of a greater research agenda on transparency and privacy in AI, and the authors have initiated several discussions with researchers working on AI governance. The tradeoff between privacy and explainability is not new to the legal landscape [7]; we are in fact optimistic about finding model explanation methods that do not violate user privacy, though this will likely come at a cost to explanation quality.

Finally, we hope that this work sheds further light on what constitutes a *good* model explanation. The recent wave of research on model explanations has been recently criticized for lacking a focus on actual usability [20], and for being far from what humans would consider helpful. It is challenging to mathematically capture human perceptions of explanation quality. However, our privacy perspective does shed some light on when explanations are not useful: explanations that offer no information on the model are likely to be less human usable (note that from our privacy perspective, we do not want private user information to be revealed, but revealing some model information is acceptable).

---

[5]See, for example, the white paper by the European Commission on Artificial Intelligence — A European approach to excellence and trust: `https://ec.europa.eu/info/sites/info/files/commission-white-paper-artificial-intelligence-feb2020_en.pdf`

References

[1] M Abadi, A Chu, I Goodfellow, H B McMahan, I Mironov, K Talwar, and L Zhang. Deep learning with differential privacy. In *Proceedings of the 23rd ACM SIGSAC Conference on Computer and Communications Security (CCS)*, pages 308–318, 2016.

[2] P Adler, C Falk, S A Friedler, G Rybeck, C Scheidegger, B Smith, and S Venkatasubramanian. Auditing black-box models for indirect influence. *Knowledge and Information Systems*, 54: 95–122, 2018.

[3] M Alber, S Lapuschkin, P Seegerer, M Hägele, K T Schütt, G Montavon, W Samek, K Müller, S Dähne, and P Kindermans. iNNvestigate neural networks! *arXiv preprint arXiv:1808.04260*, 2018.

[4] M Ancona, E Ceolini, C Öztireli, and M Gross. Towards better understanding of gradient-based attribution methods for Deep Neural Networks. In *Proceedings of the 6th International Conference on Learning Representations (ICLR)*, pages 1–16, 2018.

[5] M Ancona, E Ceolini, C Öztireli, and M Gross. Gradient-based attribution method. In *Explainable AI: Interpreting, Explaining and Visualizing Deep Learning*, pages 169–191. 2019.

[6] D Baehrens, T Schroeter, S Harmeling, M Kawanabe, K Hansen, and K Mueller. How to Explain Individual Classification Decisions. *Journal of Machine Learning Research*, 11:1803–1831, 2009.

[7] D Banisar. The right to information and privacy: Balancing rights and managing conflicts. *World Bank Institute Governance Working Paper*, 2011. URL https://ssrn.com/abstract=1786473.

[8] M Belkin and P Niyogi. Laplacian eigenmaps for dimensionality reduction and data representation. *Neural computation*, 15(6):1373–1396, 2003.

[9] M Brand. Charting a manifold. In *Proceedings of the 17th Annual Conference on Neural Information Processing Systems (NIPS)*, pages 985–992, 2003.

[10] N Carlini, C Liu, J Kos, Ú Erlingsson, and D Song. The Secret Sharer: Measuring Unintended Neural Network Memorization & Extracting Secrets. *arXiv preprint arXiv:1802.08232*, 2018.

[11] J Daligault and S Thomassé. On finding directed trees with many leaves. In *Parameterized and Exact Computation*, pages 86–97, 2009.

[12] A Datta, A Datta, A D Procaccia, and Y Zick. Influence in Classification via Cooperative Game Theory. In *Proceedings of the 24th International Joint Conference on Artificial Intelligence (IJCAI)*, pages 511–517, 2015.

[13] A Datta, S Sen, and Y Zick. Transparency via Quantitative Input Influence. In *Proceedings of the 37th IEEE Conference on Security and Privacy (Oakland)*, pages 598–617, 2016.

[14] A Datta, M Fredrikson, G Ko, P Mardziel, and S Sen. Use Privacy in Data-Driven Systems: Theory and Experiments with Machine Learnt Programs. In *Proceedings of the 24th ACM SIGSAC Conference on Computer and Communications Security (CCS)*, pages 1193–1210, 2017.

[15] D Dua and C Graff. UCI machine learning repository, 2017. URL http://archive.ics.uci.edu/ml.

[16] C Dwork, A Smith, T Steinke, and J Ullman. Exposed! a survey of attacks on private data. *Annual Review of Statistics and Its Application*, 4:61–84, 2017.

[17] C Fefferman and H Mitter, Sand Narayanan. Testing the manifold hypothesis. *Journal of the American Mathematical Society*, 29(4):983–1049, 2016.

[18] J Gilmer, L Metz, F Faghri, S S Schoenholz, M Raghu, M Wattenberg, and I Goodfellow. Adversarial spheres. *arXiv preprint arXiv:1801.02774*, 2018.

[19] B Goodman and S R Flaxman. European Union Regulations on Algorithmic Decision-Making and a "Right to Explanation". *AI Magazine*, 38(3):50–57, 2017.

[20] H Kaur, H Nori, S Jenkins, R Caruana, H Wallach, and J Wortman Vaughan. Interpreting interpretability: Understanding data scientists' use of interpretability tools for machine learning. In *Proceedings of the 2020 CHI Conference on Human Factors in Computing Systems (CHI)*, pages 1–14, 2020.

[21] F Klauschen, K Müller, A Binder, G Montavon, W Samek, and S Bach. On Pixel-Wise Explanations for Non-Linear Classifier Decisions by Layer-Wise Relevance Propagation. *Plos One*, 2015.

[22] P W Koh and P Liang. Understanding Black-box Predictions via Influence Functions. In *Proceedings of the 34th International Conference on Machine Learning (ICML)*, pages 1885–1894, 2017.

[23] A Krizhevsky and G Hinton. Learning multiple layers of features from tiny images. Technical report, 2009.

[24] Alex Krizhevsky, Ilya Sutskever, and Geoffrey E Hinton. Imagenet classification with deep convolutional neural networks. In *Proceedings of the 26th Annual Conference on Neural Information Processing Systems (NIPS)*, pages 1097–1105, 2012.

[25] I E Kumar, S Venkatasubramanian, C Scheidegger, and S Friedler. Problems with shapley-value-based explanations as feature importance measures. *arXiv preprint arXiv:2002.11097*, 2020.

[26] Y Long, V Bindschaedler, and C A Gunter. Towards measuring membership privacy. *arXiv preprint arXiv:1712.09136*, 2017.

[27] S Milli, L Schmidt, A D Dragan, and M Hardt. Model Reconstruction from Model Explanations. In *Proceedings of the 1st ACM Conference on Fairness, Accountability, and Transparency (ACM FAT*)*, pages 1–9, 2019.

[28] H Narayanan and S Mitter. Sample complexity of testing the manifold hypothesis. In *Proceedings of the 24th Annual Conference on Neural Information Processing Systems (NIPS)*, pages 1786–1794, 2010.

[29] M Nasr, R Shokri, and A Houmansadr. Machine Learning with Membership Privacy using Adversarial Regularization. In *Proceedings of the 25th ACM SIGSAC Conference on Computer and Communications Security (CCS)*, pages 634–646, 2018.

[30] N Papernot, S Song, I Mironov, A Raghunathan, K Talwar, and Ú Erlingsson. Scalable Private Learning with PATE. In *Proceedings of the 6th International Conference on Learning Representations (ICLR)*, pages 1–34, 2018.

[31] F.A.P. Petitcolas. Kerckhoffs' principle. In H.C.A. van Tilborg and Jajodia S., editors, *Encyclopedia of Cryptography and Security*. 2011.

[32] M T Ribeiro, S Singh, and C Guestrin. Why Should I Trust You?: Explaining the Predictions of Any Classifier. In *Proceedings of the 22nd International Conference on Knowledge Discovery and Data Mining (KDD)*, pages 1135–1144, 2016.

[33] O Russakovsky, J Deng, H Su, J Krause, S Satheesh, S Ma, Z Huang, A Karpathy, A Khosla, M Bernstein, A C Berg, and L Fei-Fei. ImageNet Large Scale Visual Recognition Challenge. *International Journal of Computer Vision*, 115(3):211–252, 2015.

[34] A Sablayrolles, M Douze, Y Ollivier, C Schmid, and H Jégou. White-box vs Black-box: Bayes Optimal Strategies for Membership Inference. In *Proceedings of the 36th International Conference on Machine Learning (ICML)*, pages 5558–5567, 2019.

[35] R Shokri, M Stronati, C Song, and V Shmatikov. Membership Inference Attacks Against Machine Learning Models. In *Proceedings of the 38th IEEE Conference on Security and Privacy (Oakland)*, pages 3–18, 2017.

[36] A Shrikumar, P Greenside, and A Kundaje. Not just a black box: Learning Important Features Through Propagating Activation Differences. *arXiv preprint arXiv:1605.01713*, 2017.

[37] A Shrikumar, P Greenside, and A Kundaje. Learning Important Features Through Propagating Activation Differences. In *Proceedings of the 34th International Conference on Machine Learning (ICML)*, pages 3145–3153, 2017.

[38] K Simonyan, A Vedaldi, and A Zisserman. Deep Inside Convolutional Networks: Visualising Image Classification Models and Saliency Maps. *arXiv preprint arXiv:1312.6034*, 2013.

[39] S Singh, M T Ribeiro, and C Guestrin. Programs as Black-Box Explanations. *arXiv preprint arXiv:1611.07579*, 2016.

[40] D Slack, S Hilgard, E Jia, S Singh, and H Lakkaraju. Fooling lime and shap: Adversarial attacks on post hoc explanation methods. In *Proceedings of the 3rd AAAI/ACM Conference on AI, Ethics, and Society (AIES)*, pages 180–186, 2020.

[41] J Sliwinski, M Strobel, and Y Zick. Axiomatic Characterization of Data-Driven Influence Measures for Classification. In *Proceedings of the 33rd AAAI Conference on Artificial Intelligence (AAAI)*.

[42] Daniel Smilkov, Nikhil Thorat, Been Kim, Fernanda Viegas, and Martin Winterberg. Smooth-Grad : removing noise by adding noise. *arXiv preprint arXiv:1706.03825*, 2017.

[43] L Song, R Shokri, and P Mittal. Privacy risks of securing machine learning models against adversarial examples. In *Proceedings of the 26th ACM SIGSAC Conference on Computer and Communications Security (CCS)*, pages 241–257, 2019.

[44] J T Springenberg, A Dosovitskiy, T Brox, and M Riedmiller. Striving for Simplicity: The All Convolutional Net. *arXiv preprint arXiv:1412.6806*, 2014.

[45] B. Strack, J. P. Deshazo, C. Gennings, J. L. Olmo, S. Ventura, K. J. Cios, and J. N. Clore. Impact of HbA1c measurement on hospital readmission rates: Analysis of 70,000 clinical database patient records. *BioMed Research International*, 2014, 2014.

[46] M Sundararajan and A Najmi. The many shapley values for model explanation. *arXiv preprint arXiv:1908.08474*, 2019.

[47] M Sundararajan, A Taly, and Q Yan. Axiomatic Attribution for Deep Networks. In *Proceedings of the 34th International Conference on Machine Learning (ICML)*, pages 3319–3328, 2017.

[48] S. Yeom, I. Giacomelli, M. Fredrikson, and S. Jha. Privacy risk in machine learning: Analyzing the connection to overfitting. In *2018 IEEE 31st Computer Security Foundations Symposium (CSF)*, pages 268–282, 2018.

A Detailed description of backpropagation-experiments

A.1 General setup

This is a detailed description for the setup of the experiments in Section 3. For all datasets we first create one big dataset by merging the original training and test set, to have a bigger dataset to sample from. Then we randomly sample four smaller datasets that are not overlapping and use them to train and test four target models and conduct four attacks, the other three models can respectively be used as shadow models. We repeat this process 25 times, having 100 attacks in total for each original dataset. Each small dataset is split 50/50 into training set and testing set i.e.knowing the small dataset a attacker has an a priori belief that 50% of the points are members of the training set, which is the common setting for this type of attack [35].

A.2 Target datasets and architectures

The overview of the datasets is provided in Table 3.

Name	Points	Features	Type	# Classes
Purchase	197,324	600	Binary	100
Texas	67,330	6,170	Binary	100
CIFAR-100	60,000	3,072	32×32 image	100
CIFAR-10	60,000	3,072	32×32 image	10
Hospital	101,766	127	Mixed	2
Adult	48,842	24	Mixed	2

Table 3: Overview of the target datasets for membership inference

A.2.1 Purchase dataset

The dataset originated from the "Acquire Valued Shoppers Challenge" on Kaggle[6]. The goal of the challenge was to use customer shopping history to predict shopper responses to offers and discounts. For the original membership inference attack, Shokri et al. [35] create a simplified and processed dataset, which we use as well. Each of the 197,324 records corresponds to a customer. The dataset has 600 binary features representing customer shopping behavior. The prediction task is to assign customers to one of 100 given groups (the labels). This learning task is rather challenging, as it is a multi-class learning problem with a large number of labels; moreover, due to the relatively high dimension of the label space, allowing an attacker access to the prediction vector — as is the case in [35] — represents significant access to information. We sub-sampled smaller datasets of 20,000 points i.e. 10,000 training and testing points for each model. We use the same architecture as [29], namely a four-layer fully connected neural network with $\tanh$ activations. The layer sizes are [1024, 512, 256, 100]. We trained the model of 50 epochs using the Adagrad optimizer with a learning rate of 0.01 and a learning rate decay of 1e-7.

A.2.2 Texas hospital stays

The Texas Department of State Health Services released hospital discharge data public use files spanning from 2006 to 2009.[7] The data is about inpatient status at various health facilities. There are four different groups of attributes in each record: general information (e.g. hospital id, length of stay, gender, age, race), the diagnosis, the procedures the patient underwent and the external causes of injury. The goal of the classification model is to predict the patient's primary procedures based on the remaining attributes (excluding the secondary procedures). The dataset is filtered to include only the 100 most common procedures. The features are transformed to be binary resulting in 6,170 features and 67 330 records. We sub-sampled smaller datasets of 20,000 points i.e. 10,000 training and testing points for each model. As the dataset has only 67,330 points we allowed resampling of points. We use the same architecture as [29], namely a five-layer fully connected neural network with $\tanh$ activations. The layer sizes are [2048, 1024, 512, 256, 100]. We trained the model of 50 epochs using the Adagrad optimizer with a learning rate of 0.01 and a learning rate decay of 1e-7.

---

[6]https://www.kaggle.com/c/acquire-valued-shoppers-challenge/data
[7]https://www.dshs.texas.gov/THCIC/Hospitals/Download.shtm

A.2.3 CIFAR-10 and CIFAR-100

CIFAR-10 and CIFAR-100 are a well known benchmark datasets for image classification [23]. They consists of 10 (100) classes of $32 \times 32 \times 3$ color images, with 6,000 (600) images per class. The datasets are usually split in 50,000 training and 10,000 test images. For CIFAR-10, we use a small convolutional network with the same architecture as in [35, 34], it has two convolutional layers with max pooling, and to dense layers, all with Tanh activations. We train the model for 50 epochs with a learning rate of 0.001 and the Adam optimizer. Each dataset has 30,000 points (i.e. 15,000 for training). Hence, we only have enough points to train one shadow model per target model. For CIFAR-100, we use a version of Alexnet [24], it has five convolutional layers with max pooling, and to dense layers, all with ReLu activations. We train the model for 100 epochs with a learning rate of 0.0001 and the Adam optimizer. Each dataset has 60,000 points (i.e. 30,000 for training). Hence, we don't have enough points to train shadow models.

A.2.4 UCI Adult (Census income)

This dataset is extracted from the 1994 US Census database [15]. It contains 48,842 datapoints and based on 14 features (e.g. age, workclass, education) the goal is to predict if the yearly income of a person is above 50,000 \$. We transform the categorical features into binary form resulting in 104 features. We sub-sampled smaller datasets of 5,000 points i.e. 2,500 training and testing points for each model. As architecture we use a five-layer fully connected neural network with Tanh activations. The layer sizes are [20, 20, 20, 20, 2]. We trained the model of 20 epochs using the Adagrad optimizer with a learning rate of 0.001 and a learning rate decay of 1e-7.

A.2.5 Diabetic Hospital

The dataset contains data on diabetic patients from 130 US hospitals and integrated delivery networks [45]. We use the modified version described in [22] where each patient has 127 features which are demographic (e.g. gender, race, age), administrative (e.g., length of stay) and medical (e.g., test results); the prediction task is readmission within 30 days (binary). The dataset contains 101,766 records from which we sub-sample balanced datasets of size 10,000 (i.e. with equal numbers of patients from each class). Since the original dataset is heavily biased we don't have enough points to train shadow models. As architecture we use a four-layer fully connected neural network with Tanh activations. The layer sizes are [1024, 512, 256, 100]. We trained the model for 1,000 epochs using the Adagrad optimizer with a learning rate of 0.001 and a learning rate decay of 1e-6.

B   Results for other backpropagation-based explanations

Besides the gradient, several other explanation methods based on backpropagation have been proposed. We conducted the attack described in Section 2.2 replacing the gradient with some other popular of these explanation methods. The techniques below are all implemented in the INNVESTIGATE library[8] [3]. A in depth discussion of some of these measures and the relations between them can also be found in [4].

Integrated Gradients   Sundararajan et al. [47] argue that instead of focusing on the gradient it is better to compute the average gradient on a linear path to a baseline $\vec{x}_{BL}$ (often $\vec{x}_{BL} = \vec{0}$). This approach satisfies three desirable axioms: sensitivity, implementation invariance and a form of completeness. Sensitivity means that given a point $\vec{x} \in \mathcal{X}$ such that $x_i \neq x_{BL,i}$ and $c(\vec{x}) \neq c(\vec{x}_{BL})$, then $\phi_i(\vec{x}) \neq 0$; completeness means that $\sum_{i=1}^{n} \phi_i(\vec{x}) = c(\vec{x}) - c(\vec{x}_{BL})$. Mathematically the explanation can be formulated as

$$\phi_{INTGRAD}(\vec{x})_i \triangleq (x_i - \vec{x}_{BL,i}) \cdot \int_{\alpha=0}^{1} \left. \frac{\partial c(\vec{x}^{\alpha})}{\partial \vec{x}_i^{\alpha}} \right|_{\vec{x}^{\alpha} = \vec{x} + \alpha(\vec{x} - \vec{x}_{BL})} .$$

Guided Backpropagation   Guided Backpropagation [44] is a method specifically designed for networks with ReLu activations. It is a modified version of the gradient where during backpropagation only paths are taken into account that have positive weights and positive ReLu activations. Hence, it

---

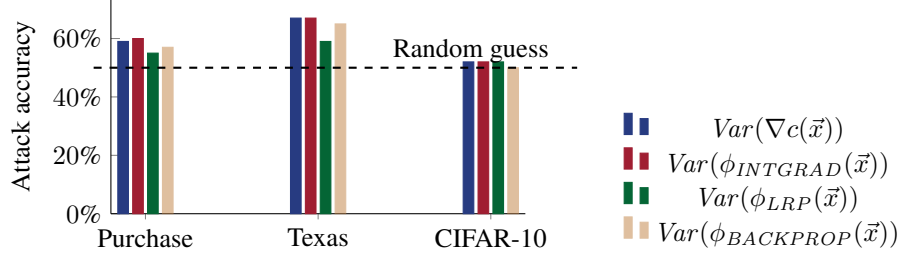[8]https://github.com/albermax/innvestigate

Figure 3: Results for the threshold-based attacks using different backpropagation-based explanations as sources of information for the attacker.

only considers positive evidence for a specific prediction. While being designed for ReLu activations it can also be used for networks with other activations.

Layer-wise Relevance Propagation (LRP)   Klauschen et al. [21] use backpropagation to map *relevance* back from the output layer to the input features. Let l be a layer in the network and the number of layers be denoted by L. Then the relevance $r_i^{(l)}$ of the i-th neuron in the l-th layer can be computed as:

$$r_i^{(L)}(\vec{x}) \triangleq c_i(\vec{x})$$
$$r_i^{(l)}(\vec{x}) \triangleq \sum_j \frac{z_{ji}}{\sum_{i'}(z_{ji'} + b_j) + \epsilon \cdot \text{sign}(\sum_{i'}(z_{ji'} + b_j))} r_j^{(l+1)}$$

Here z_{ji} is the weighted activation of neuron i to neuron j in the next layer and b_j is the bias added to neuron j. The summations are over all neurons in the respective layers. Finally, the ϵ is added to avoid numerical instabilities. In words, LRP defines the relevance in the last layer as the output itself and in each previous layer the relevance is redistributed according to the weighted contribution of the neurons in the previous layer to the neurons in the current layer. The final attributions for the input $\vec{x}$ are defined as the attributions of the input layer: $\phi_{LRP}(\vec{x})_i \triangleq r_i^{(1)}(\vec{x})$.

Evaluation   As can be seen in Figure 3 on the Purchase, Texas and CIFAR-10 datasets, the results for other backpropagation based methods are relatively similar to the attack based on the gradient. Integrated gradients being most similar to the gradient. We omitted Adult, Hospital and CIFAR-100 to save some computations as some small tests indicated that the results would be comparably bad as for attacks based on the gradient.

C   The Influence of the Input Dimension

The experiments in Section 3 indicate that $Var(\nabla c(\vec{x}))$, and $||\nabla c(\vec{x})||_1$ predict training set membership. In other words, high absolute gradient values at a point $\vec{x}$ signal that $\vec{x}$ is *not* part of the training data: the classifier is uncertain about the label of $\vec{x}$, paving the way towards a potential attack. Let us next study this phenomenon on synthetic datasets, and the extent to which an adversary can exploit model gradient information in order to conduct membership inference attacks. The use of artificially generated datasets offers us control over the problem complexity, and helps identify important facets of information leaks.

To generate datasets, we use the Sklearn python library.[9] For n features, the function creates an n-dimensional hypercube, picks a vertex from the hypercube as center of each class, and samples points normally distributed around the centers. In our experiments, the number of classes is either 2 or 100 while the number of features is between 1 to 10,000 in the following steps,

$$n \in \{1, 2, 5, 10, 14, 20, 50, 100, 127, 200, 500, 600,$$
$$1000, 2000, 3072, 5000, 6000, 10000\}.$$

---

[9]the `make_classification` function `https://scikit-learn.org/stable/modules/generated/sklearn.datasets.make_classification.html`
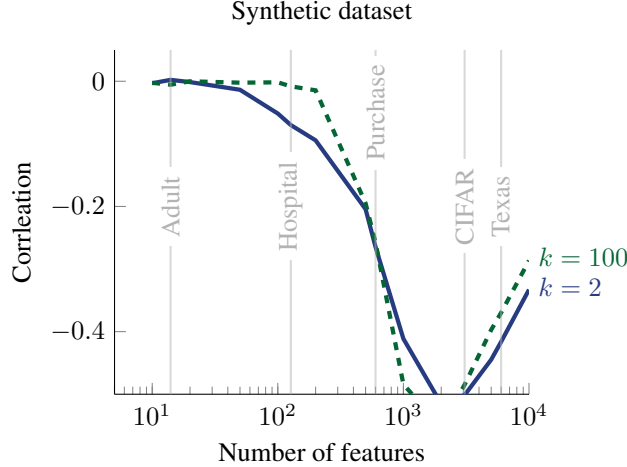
Figure 4: The correlation between $||\nabla c(\vec{x})||_1$ and training membership for synthetic datasets for increasing number of features n and different number of classes $k \in \{2, 100\}$

For each experiment, we sample 20,000 points and split them evenly into training and test set. We train a fully connected neural network with two hidden layers with fifty nodes each, the $\texttt{tanh}$ activation function between the layers, and softmax as the final activation. The network is trained using Adagrad with learning rate of 0.01 and learning rate decay of $1\mathrm{e}-7$ for 100 epochs. Figure 5 contains an illustration of the generated data.

Increasing the number of features does not increase the complexity of the learning problem as long as the number of classes is fixed. However, the dimensionality of the hyper-plane increases, making its description more complex. Furthermore, for a fixed sample size, the dataset becomes increasingly sparse, potentially increasing the number of points close to a decision boundary. Increasing the number of classes increases the complexity of the learning problem.

Figure 4 shows the correlation between $||\nabla c(\vec{x})||_1$ and training membership. For datasets with a small number of features ($\leq 10^2$) there is almost no correlation. This corresponds to the failure of the attack for Adult and the Hospital dataset. When the number of features is in the range ($10^3 \sim 10^4$) there is a correlation, which starts to decrease when the data dimension is further increased. The number of classes seems to play only a minor role; however, a closer look at training and test accuracy reveals that the actual behavior is quite different. For two classes and a small number of features training and testing accuracy are both high (almost 100%), around $n = 10^2$ the testing accuracy starts to drop (the model overfits) and at $n = 10^3$ the training accuracy starts to drop as well reducing the overfitting. For 100 classes the testing accuracy is always low and only between $10^3 \leq n \leq 10^4$ the training accuracy is high, leading to overfitting, just on a lower level. We also conduct experiments with networks of smaller/larger capacity, which have qualitatively similar behavior. However, the interval of n in which correlation exists and the amount of correlation varies (see Figure 6).

D   Considering the entire explanation vector

The attacks described in Section 2.2 use only the variance of the explanation as information to create an attack. Shokri et al. [35] describe an attack that can take the entire explanation vector as an input.

The fundamental idea is to cast membership inference as a *learning problem*: the attacker trains an *attack model* that, given the output of a *target model* can predict whether the point $\vec{x}$ was used during the training phase of c. The main drawback of this approach is that it assumes that the attacker has partial knowledge of the initial training set in order to train the attack model. Shokri et al. [35] circumvent this by training *shadow models* (i.e. models that mimic the behavior of c on the data), and demonstrate that comparable results can be obtained even when the attacker does not have access to parts of the initial training set. As we compare the results to the optimal threshold it is appropriate to compare with a model that is trained using parts of the actual dataset, to allow for a stronger attack.
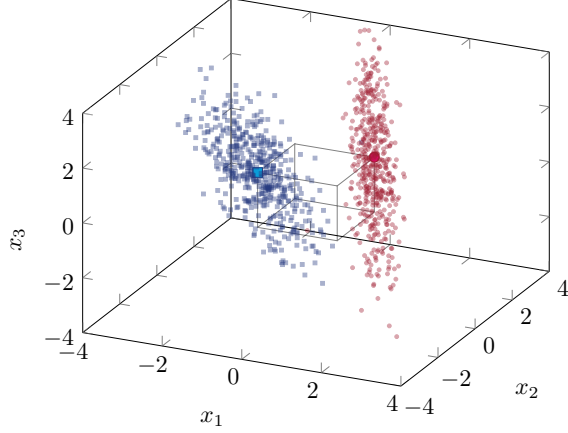
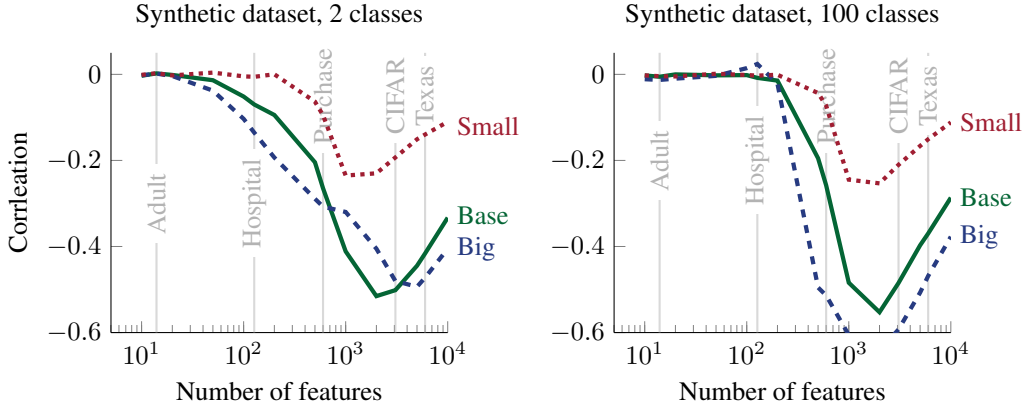Figure 5: An illustration of the dataset generation process with $n = 3$.

Figure 6: The correlation between $||\nabla c(\vec{x})||_1$ and training membership for synthetic datasets for increasing number of features n and different number of classes $k \in \{2, 100\}$ for three different networks. The "Small" has one hidden layer with 5 nodes, "Base" has two layers with 50 nodes each, "Big" has 3 layers with 100 nodes each.

The specific attack architecture, we use in this section, is a neural network inspired by the architecture of Shokri et al. [35]. The network has fully connected layers of sizes $[r, 1024, 512, 64, 256, 64, 1]$, where r is the dimension of the respective explanation vector. We use ReLu activations between layers and initialize weights in a manner similar to Shokri et al. [35] to ensure a valid comparison between the methods. We trained the attack model for 15 epochs using the Adagrad optimizer with a learning rate 0.01 of and a learning rate decay of 1e-7. As data for the attacker we used 20,000 explanations generated by the target 10,000 each for members and non-members. The training testing split for the attacker was 0.7 to 0.3. We repeated the experiment 10 times. We omitted CIFAR-100 for computational reasons.

As can be seen in Figure 7 attacks based on the entire explanation perform slightly better than attacks based only on the variance. However, they are qualitatively the same and still perform very poorly for CIFAR-10, Adult and Hospital.

E   Influence of overfitting

To study the influence of overfitting on the success of membership inference attacks based on backpropagation-based methods, we trained models for varying epochs, which leads to varying gaps between training and testing accuracy. We used the same settings as for the experiments in Section 3 as described in Appendix A. With the exception of the number of epochs we trained each target model, which we varied from 5 to 50 in steps 5. For each number of epochs we trained 20 target
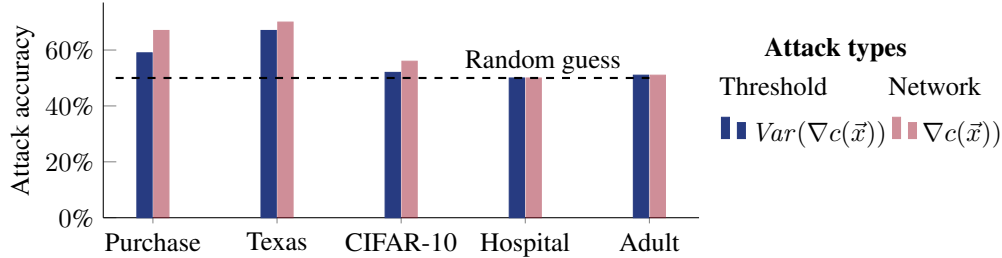
Figure 7: A comparison between attacks using only the variance of the gradient and attacks using the entire gradient explanation as input.
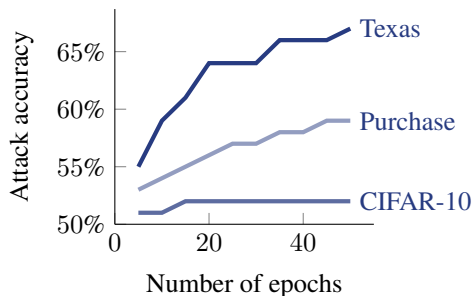

Figure 8: The attack accuracy of the attacker increases with increasing number of epochs.

models. We only report the results for the optimal attack, as shadow model based attacks are similar. We only conducted experiments for Purchase, Texas, and CIFAR-10 where we had positive results for the highest amount of overfitting, which is achieved in the original setting.

F   Attacks using Lime explanation

We ran additional experiments where the attacker has access to the Lime [39] explanations. The type of attack is the same as described in Section 2.2 (i.e. we use an optimal threshold based on the variance of the explanation). However, the calculation of Lime explanations takes considerably longer than the other explanations we considered. Each single explanation computes for a couple of seconds. Running experiments with 10,000 or more explanations would take weeks to months. To save time and energy we decided to run only some smaller scale experiments where the models are trained on 1,000 points and the attacks run on 2,000 points each (1,000 members and 1,000 non-members), we also repeated each experiment only 20 times instead of 100 as for the others. As the experiments for the other explanations indicated that only for Purchase and Texas the attack was likely to be successful we restricted our experiments to these two datasets. Figure 9 shows the results for these attacks, we also rerun the attacks for the gradient and SmoothGrad explanations, as well as the attack using the prediction variance in this new setting, to ensure that it's not the different setting that determines the outcome. Neither, Lime nor SmoothGrad outperform random guessing. For the Purchase dataset, however, the attack using the gradient variance fails as well. As a final interesting observation, we are unable to explain at the moment, for the Texas dataset the gradient based attack actually performs better than on the larger dataset (shown in Figure 1) it even outperforms the attack based on the prediction in this specific setting. Something we want to explore further in future works.

G   Membership inference for example-based explanations

In this section we give a detailed description of the experiments for membership inference using example-based explanations.
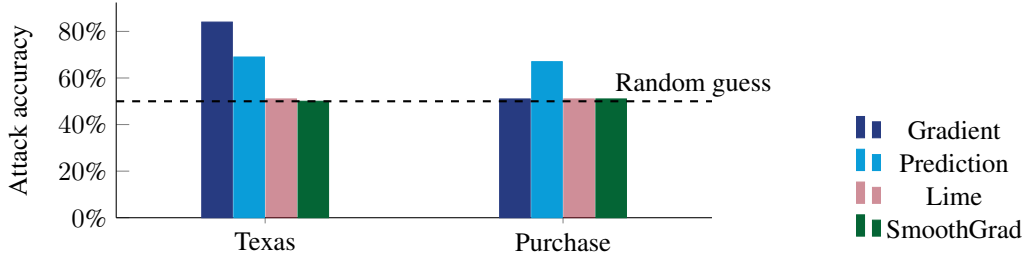
Figure 9: Attacks using Lime or SmoothGrad do not outperform random guessing in any of our experiments.
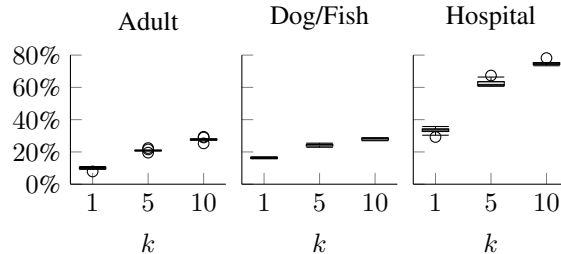

Figure 10: % of training points revealed as their own explanation, when $k \in \{1, 5, 10\}$ most influential points are revealed.

G.1 Experimental setup

While the theoretical framework of influence functions described in Section 2 can be applied to an arbitrary classification task, it requires the training of as many classifiers as there are points in the training set in practice. Koh and Liang [22] propose an approximation method, but currently we only have access of its implementation for binary logistic regression models. However, for logistic regression, retraining the model (i.e. computing an *exact solution*) is actually faster than running the approximation algorithm. For larger models and datasets, these explanation methods seems intractable at the moment. This limits our experiments to the Adult and Hospital datasets from our previous experiments for which we train binary logistic regression models. Furthermore, given the relatively long time it takes to compute all models, we reduce the size of the training set to 2,000 points, so we can run one experiment within a few hours (see Figure 11 for an exploration of the effect of dataset size). Koh and Liang [22] use a specifically created dataset containing 2400 299×299-pixel dog and fish images, extracted from ImageNet [33]. The images were pre-processed by taking the output of the penultimate layer of a neural network trained on ImageNet.[10] These latent representations were then used to train a linear regression model. For more variety we include this dataset here as the *Dog/Fish* dataset. Arguably, this dataset doesn't contain particularly private information, but it can be seen as representative of image data in general. It also allows us to attack a pre-trained deep neural network which last layer was fine tuned. This type of transfer learning for small dataset becomes increasingly popular. Given the small size of this dataset we randomly split it into 1800 training and 600 test points for each experiment. For each dataset we repeat the experiment 10 times.

G.2 Evaluation

Figure 10 shows the percentage of training points that would be revealed by explaining themselves. For the standard setting where the top 5 most influential points are revealed, a quarter of each dataset is revealed on average. For the Hospital dataset, two thirds of training points are revealed. Even when just the most influential point would be released for the Adult dataset (which exhibits the lowest success rates), 10% of the members are revealed through this simple test.

---

[10]Specifically, the authors used an Inceptionv3 architecture, for which pre-trained models are available for Keras https://keras.io/applications/#inceptionv3.
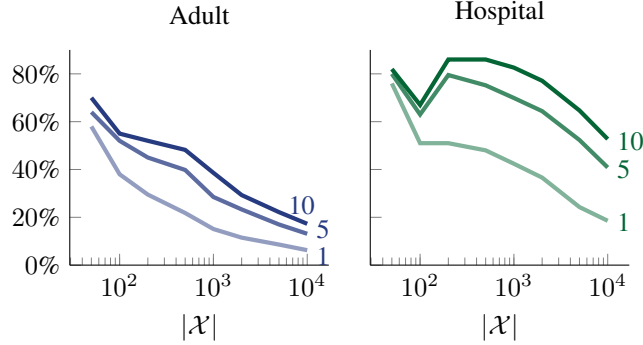
Figure 11: % of k-self-revealing points depending on the size of the dataset ($|\mathcal{X}|$) for $k \in \{1, 5, 10\}$ Increasing datasize the relative number of self-revealing points decreases. However, the decrease is relatively slow (the figure is in logarithmic scale) and the absolute number of revealed points is actually increasing.
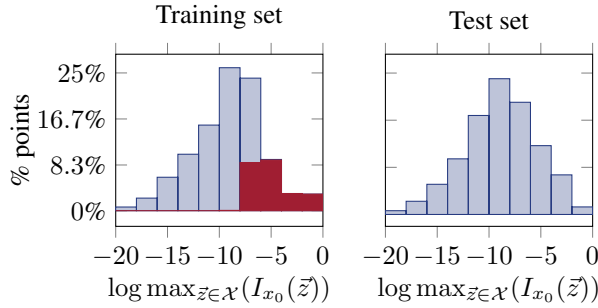

Figure 12: Histogram of the influence of the most influential points for every point in the training set(left) and test set (right) on a logarithmic scale (for one instance of Dog/Fish). The points in the training set for which the membership inference is successful (i.e. $\vec{x}_0 = \mathrm{argmax}_{\vec{z} \in \mathcal{X}}(I_{x_0}(\vec{z}))$) are highlighted in red (dark).

As mentioned in Section 2.1.2, the influence score of the most influential points might be released to a user as well. In our experiments, the influence scores are similarly distributed between training and test points (i.e. members and non-members); however, the distribution is significantly different once we ignore the revealed training points. Figure 12 illustrates this for one instance of the Dog/Fish dataset; similar results hold for the other datasets. An attacker can exploit these differences, using techniques similar to those discussed in Section 2.2; however, we focus on other attack models in this work.

Minority and Outlier Vulnerability to Inference Attacks   Before turning our attention to dataset reconstruction attacks, we highlight an interesting finding. Visual inspection of datapoints for which membership attacks were successful indicates that outliers and minorities are more susceptible to being part of the explanation. Images of animals (a bear, a bird, a beaver) eating fish (and labeled as such) were consistently revealed (as well as a picture containing a fish as well as a (more prominent) dog that was labeled as fish). We label three "minorities" in the dataset to test the hypothesis that pictures of minorities are likelier to be revealed (Table 4a).

With the exception of $k = 1$ (for lion and clown fish), minorities are likelier to be revealed. While clownfish (which are fairly "standard" fish apart from their distinct coloration) exhibit minor differences from the general dataset, birds are more than three times as likely to be revealed. The Hospital dataset exhibits similar trends (Table 4b). Young children, which are a small minority in the dataset, are revealed to a greater degree; ethnic minorities also exhibit slightly higher rates than Caucasians. This is mirrored (Table 4c) for the Adult dataset, with the exception of the age feature and the "Black" minority. Young people are actually particularly safe from inference. Note however, that young age is a highly predictive attribute for this classification. Only 3 out of the 2,510 entries aged younger than 20 have an income of more than 50K and none of them made it in any of our training set. Similarly only 12% of the Black people in the dataset (vs. 25% over all) have a positive label, making this attribute more predictive an easier to generalize.

	#points	$k=1$	$k=5$	$k=10$
Whole dataset	100%	16%	24%	28%
Birds	0.6%	64%	84%	86%
Clownfish	1%	14%	30%	33%
Lion fish	1%	9%	31%	43%

(a) Disclosure likelihood by type in the Dog/Fish dataset.

	% of data	$k=1$	$k=5$	$k=10$
Whole dataset	100%	33%	63%	75%
Age 0 -10	0.2%	61%	100%	100%
Age 10 -20	0.7%	23%	62%	95%
Caucasian	75%	32%	62%	74%
African American	19%	36%	66%	78%
Hispanics	2%	40%	61%	77%
Other race	1.5%	30%	60%	79%
Asian American	0.6%	33%	70%	95%

(b) Disclosure likelihood by age and race in the Hospital dataset.

	% of data	$k=1$	$k=5$	$k=10$
Whole dataset	100%	10%	21%	28%
Age 10 -20	5%	0%	1%	1%
White	86%	10%	21%	28%
Black	10%	9%	16%	19%
Amer-Indian-Eskimo	1%	8%	23%	32%
Other	0.8%	16%	32%	43%
Asian-Pac-Islander	3.%	21%	40%	48%

(c) Disclosure likelihood by age and race in the Adult dataset.

Table 4: Minority populations are more vulnerable to being revealed by the Koh and Liang method.

While our findings are preliminary, they are quite troubling in the authors' opinion: transparency reports aim, in part, to *protect* minorities from algorithmic bias; however, data minorities are exposed to privacy risks through their implementation. Our findings can be explained by earlier observations that training set outliers are likelier to be "memorized" and thus less generalized [10]; however, such memorization leaves minority populations vulnerable to privacy risks.

H Dataset reconstruction for example-based explanations

This section describes ou proposed attack models for dataset reconstruction based on example-based model explanations.

Given a parameter $\theta = (\vec{w}, b) \in \mathbb{R}^n \times \mathbb{R}$ a logistic regression model is defined as

$$f_\theta(\vec{x}) = \frac{1}{1 + e^{-\vec{w}^T \vec{x} + b}}.$$

For a point $\vec{y} \in R^n$ with label $l(\vec{y}) \in \{0, 1\}$ we define the loss of $f(\vec{y})_\theta$ as

$$L(\vec{y}, \theta) = (1 - f_\theta(\vec{y}))^{l(\vec{z})} (f_\theta(\vec{y}))^{1 - l(\vec{z})},$$

which corresponds to the standard maximal likelihood formulation. As logistic regression does not allow for a closed form optimum, it is generally trained via gradient ascent. We assume we are given a fixed training regime A (i.e. fixed parameters for number of steps, learning rate etc.).

Let f_θ be the model induced by $\mathcal{X}$ and

$$\mathcal{F}_\mathcal{X} = \{f_{\theta_{\vec{x}}} | f_{\theta_{\vec{x}}} \text{ is induced by } \mathcal{X} \setminus \{\vec{z}\}, \vec{x} \in \mathcal{X}\}$$

be the set of functions induced by omitting the training points. We can reformulate the influence of point $\vec{x}$ on point $\vec{y}$ (assuming $l(\vec{y}) = 0$) as

$$I_{\vec{y}}(\vec{x}) = L(y, \theta) - L(y, \theta_{\vec{x}})$$
$$= f_\theta(y) - f_{\theta_{\vec{x}}}(y)$$
$$= \frac{1}{1 + e^{-\vec{w}^T \vec{y} + b}} - \frac{1}{1 + e^{-\vec{w}_{\vec{x}}^T \vec{y} + b_{\vec{x}}}}$$

The condition that $\vec{y}$ reveals $\vec{x}$ is thus equivalent to ensuring that for all $\vec{z} \in \mathcal{X}$, $|I_{\vec{y}}(\vec{x})| \geq |I_{\vec{y}}(\vec{z})|$. In the case of linear regression this simply implies that

$$\left| \frac{1}{1 + e^{-\vec{w}^T \vec{y} + b}} - \frac{1}{1 + e^{-\vec{w}_{\vec{x}}^T \vec{y} + b_{\vec{x}}}} \right|$$
$$\geq \left| \frac{1}{1 + e^{-\vec{w}^T \vec{y} + b}} - \frac{1}{1 + e^{-\vec{w}_{\vec{z}}^T \vec{y} + b_{\vec{z}}}} \right|$$

which can be simplified to a linear constraint (whose exact form depends on whether the terms in absolute values are positive or negative).

H.1 Algorithm to recover the training set by minimizing the influence of already discovered points

See Algorithm 1. We note that for an small enough ϵ the algorithm needs $\sum_{i=0}^{l} n - i + 1$ queries to reveal l points. In our implementation we use n queries per point to reconstruct each revealed point over $\mathbb{R}^n$ and instead of solving the set of equations exactly we solve a least squares problem to find regions with zero influence, which has greater numerical stability.

H.2 Bounds on number of revealable points

This section contains an analysis on the upper and lower number of points that can be revealed through influence-based explanation methods revealing examples as explanations. It is relatively easy to construct examples in which only two points in the dataset can be revealed (see Figure 13). In

---

Algorithm 1 Recovering the training set by minimizing the influence of already recovered points

1: linearlyIndependent ← True
2: $q \leftarrow 0$
3: $R_0 \leftarrow \mathbb{R}^n$
4: revealedVectors ← []
5: **while** linearlyIndependent **do**
6:     $\vec{y} \leftarrow$ pickRandomPointIn(R_q)
7:     $\vec{x} \leftarrow \text{argmax}_{\vec{z} \in \mathcal{X}}(|I_{\vec{y}}(\vec{z})|)$
8:     revealedVectors.append$(\vec{x})$
9:     vectorsNotFound ← getBasisOf(R_q)
10:     spanningVectors ← $[\vec{y}]$
11:     **while** vectorsNotFound $\neq \emptyset$ **do**
12:         **for** $\vec{v} \in$ vectorsNotFound **do**
13:             **if** $\vec{x} = \text{argmax}_{\vec{z} \in \mathcal{X}}(|I_{\vec{y}+\epsilon\vec{v}}(\vec{z})|)$ **then**
14:                 spanningVectors.append$(\vec{y} + \epsilon\vec{v})$
15:             **end if**
16:         **end for**
17:         $\epsilon \leftarrow \frac{\epsilon}{2}$
18:     **end while**
19:     **if** $\exists r \in \mathbb{R}: \forall \vec{v} \in$ spanningVectors: $|I_{\vec{y}+\epsilon\vec{v}}(\vec{x})| = r$ **then**
20:         linearlyIndependent ← False
21:     **else**
22:         $R_{q+1} \leftarrow \{\vec{y} \in R_q | |I_{\vec{y}}(\vec{x})| = 0\}$
23:         $q \leftarrow q + 1$
24:     **end if**
25: **end while**
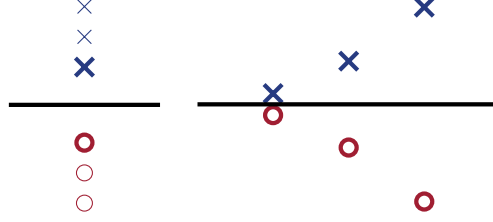26: **return** revealedVectors

---

Figure 13: Illustrations of datasets for which only two (left) or all (right) points can be revealed under standard training procedures.

fact, there are specific instances in which only a single datapoint can be revealed (see Lemma H.1), however these cases are neither particularly insightful nor do they reflect real-world settings. On the other side, there exists datasets where, independent of the number of features, the entire dataset can be recovered. The right side of Figure 13 illustrates such an example.

The following Lemma characterizes the situations in which only a single point of the dataset can be revealed for $X \subseteq \mathbb{R}$. The conditions for higher dimensions follow from this.

Lemma H.1. *Given a training set $\mathcal{X}$ let f_θ and $\mathcal{F}_\mathcal{X}$ be induced by $\mathcal{X}$ with $|\mathcal{F}_\mathcal{X}| \geq 2$, then one of the following statements is true*

1. *$\forall \vec{x} \in \mathcal{X} \colon w = w_{\vec{x}}$ and $(b \geq b_{\vec{x}}, \forall x \in \mathcal{X}) \vee (b \leq b_{\vec{x}}, \forall x \in \mathcal{X})$ (i.e all functions in $\mathcal{F}_\mathcal{X}$ are shifted in one direction of f_θ),*

2. *$\exists \vec{y} \in \mathbb{R}^n \colon \forall \vec{x} \in \mathcal{X} \colon w_{\vec{x}}\vec{y} + b_{\vec{x}} = w\vec{y} + b$ (i.e all functions in $\mathcal{F}_\mathcal{X}$ intersect with in f_θ the same point),*

3. *$\forall \vec{x} \in \mathcal{X} \colon w = w_{\vec{x}}$ and there exists a numbering of the points in $\mathcal{X}$ such that $b_1 \leq b_2 \leq \cdots \leq b_k \leq b \leq b_{k+1}, \ldots, b_m$ such that $b \leq \log(\frac{1}{2}(e^{b_1} + e^{b_m}))$.*

4. *at least two points can be revealed.*

Proof. It is easy to see that in the first two situations only one point can be revealed (the one corresponding to the largest shift or largest angle at intersection). In the third case all functions in $\mathcal{F}_\mathcal{X}$ are shifts of f_θ, but not all in the same direction. Only, the left most and right most shift are candidates for being revealed as they clearly dominate all other shifts. Also we assume $b_1 < b < b_m$ (as soon as one shift coincidences with the original model the statement is trivially true). Some calculus reveals the condition for which the two points would have the same influence is

$$y = \ln \left(\frac{-2e^b + e^{b_1} + e^{b_m}}{e^{b+b_1} + e^{b+b_m} - 2e^{b_1+b_m}} \right) / w$$

, which is well defined when the expression inside the logarithm is positive and $e^{b+b_1} + e^{b+b_m} - 2e^{b_1+b_m} \neq 0$. The former is the case for $b < \log(\frac{1}{2}(e^{b_1} + e^{b_2}))$, which also ensures the latter condition. On the other hand if $b \leq \log(\frac{1}{2}(e^{b_1} + e^{b_m}))$ the equation has no solution and so only one point can be revealed.

It remains to show that in all other cases at least two points can be revealed. Let's assume that there is a single $\vec{x} \in \mathcal{X} \colon \vec{w} \neq \vec{w}_{\vec{x}}$. In this case $w_{\vec{x}}^T \vec{y} + b_{\vec{x}} = w^T \vec{y} + b$ can be solved and at the solutions $I(\vec{x}) = 0$ yet all other points have nonzero influence and one of them is revealed. Yet, since $w_{\vec{x}'}^T \vec{y} + b_{\vec{x}} - w^T \vec{y} + b$ is constant for all $\vec{x}' \in \mathcal{X}, \vec{x} \neq \vec{x}$ and $|w_{\vec{x}}^T \vec{y} + b_{\vec{x}} - w^T \vec{y} + b|$ can take arbitrary values, there exists $\vec{y} \in R^n$ such that $\vec{x} = \operatorname{argmax}_{\vec{z} \in \mathcal{X}} |I_{\vec{y}}(\vec{z})|$. Finally, if there are multiple points with $\vec{x} \in \mathcal{X} \colon \vec{w} \neq \vec{w}_{\vec{x}}$ none of them can be revealed for all $\vec{y}$ as long as the condition in 2) is not satisfied. $\square$

The following result states that there exist models and datasets for which every point can be revealed.

Lemma H.2. *For every $m \in \mathbb{N}$ there exists a dataset $\mathcal{X} \subset \mathbb{R}^n$ with $|\mathcal{X}| = m$ and a training procedure A so that any point in $\mathcal{X}$ can be revealed by example-based explanations.*

Proof. Given that we do not have restrictions on our training procedure A the claim is equivalent to the existence of a parameter θ and a series of parameters θ_k and points y_k such that $\forall k, m \in \mathbb{N}$:

$$|L(\vec{y}_k, \theta) - L(\vec{y}_k, \theta_k)| = \max_{i \in [m]} |L(\vec{y}_k, \theta) - L(\vec{y}_k, \theta_i)|$$

W.l.o.g. $n = 1$, let $w = b = 0$ and $\forall k\colon l(y_k) = 0$, then

$$|L(\vec{y}_k, \theta) - L(\vec{y}_k, \theta_k)| = \max_{i \in [m]} |L(\vec{y}_k, \theta) - L(\vec{y}_k, \theta_i)|$$

$$\Leftrightarrow L(\vec{y}_k, \theta_k) = \max_{i \in [m]} |L(\vec{y}_k, \theta) - L(\vec{y}_k, \theta_i)$$

$$\Leftrightarrow f_{\theta_k}(\vec{y}_k) = \max_{i \in [m]} f_{\theta_i}(\vec{y}_k) \Leftrightarrow w_k y_k - b_k = \max_{i \in [m]} w_i y_k - b_i$$

The above condition is satisfied for $w_k = 2k$, $y_k = k$ and $b_k = k^2$, as this describes the series of tangents of the strictly convex x^2 function. $\qquad\square$

I Proof of Theorem 4.1

We begin by restating Theorem 4.1

Theorem 4.1. *Given a training set $\mathcal{X} \subset \mathbb{R}^n$, let $\theta = (\vec{w}, b)$ be the parameters of a logistic regression model induced by $\mathcal{X}$. Let $d \in \mathbb{N}$ be the largest number such that the vectors in $W = \{\vec{w}_{\vec{x}} | \vec{x} \in \mathcal{X}, (\vec{w}_{\vec{x}}, b_{\vec{x}}) \triangleq A(\mathcal{X} \setminus \{\vec{x}\})\}$ are d-wise linearly independent, then if all vectors in W are linearly independent of $\vec{w}$, Algorithm 1 (with query access to model predictions and example-based explanations) reveals at least d points in $\mathcal{X}$ with probability 1.*

Proof. We need to show two statements (a) given an affine subspace R_q of dimension $n - q$ in which the influence of the first $q < d$ points is zero, with probability 1 a new point is revealed and (b) Algorithm 1 constructs a new subspace R_{q+1} in which the influence of the first $q + 1$ points is zero, with probability 1.

For $q = 0$ $R_q = \mathbb{R}^n$ and statement (a) is trivially true: querying any point will reveal a new point. Now, when $q > 0$ and the attacker queries a point $\vec{y} \in R_q$, the only reason that no new point is revealed is that for all points $\vec{x} \in \mathcal{X}$ we have $I_{\vec{y}}(\vec{x}) = 0$. Note that $I_{\vec{y}}(\vec{x}) = 0$ iff $-\vec{w}^T \vec{y} + b = -\vec{w}_{\vec{x}}^T \vec{y} + b_{\vec{x}}$. Thus, if $I_{\vec{y}}(\vec{x}) = 0$ for all $\vec{x} \in \mathcal{X}$, then for all $\vec{x}_1, \vec{x}_2 \in \mathcal{X}$, $-\vec{w}_{\vec{x}_1}^T \vec{y} + b_{\vec{x}_1} = -\vec{w}_{\vec{x}_2}^T \vec{y} + b_{\vec{x}_2}$. By the d-wise independence assumption of $\vec{w}_i$ this can only happen in an $n - d$-dimensional subspace of $Z \subset \mathbb{R}^n$. The probability of sampling a point in the intersection of this subspace with R_q is 0 as $\dim(R_q \cap Z) \leq n - d < n - q = \dim(R_q)$.

To prove Statement (b) we first note that the attacker can recover θ (i.e. the original function) by querying f_θ for $n + 1$ suitable — i.e., n of these points must be linearly independent, and the last one is different but otherwise arbitrary point — points and solving the corresponding linear equations. Knowing θ, the attacker can recover $|\theta_{\vec{x}}|$ for a vector $\vec{x} \in \mathcal{X}$, given the values of $|I_{\vec{y}_i}(\vec{x})|$ for $\vec{y}_i \in \mathbb{R}^n, i \in [n + 1]$ suitable points. Similarly, the attacker can reconstruct the entire behavior of $|I_{\vec{y}_i}(\vec{x})|$ on an $n - q$ dimensional affine subspace R_q from $n - q + 1$ suitable points.

Lines 9 to 18 in Algorithm 1 find these points. Since $|I_{\vec{y}}(\vec{x})|$ is continuous, the argmax in Line 7 is constant in a small region around $\vec{y}$, as long as there is no tie. Hence, ϵ will eventually become sufficiently small so that all points $\vec{y} + \epsilon v$ reveal the same point as $\vec{y}$. If there is a tie for the argmax at $\vec{y}$, let S be a open set of points around $\vec{y}$ such that $\forall \vec{y}' \in S \colon |\operatorname{argmax}_{\vec{z} \in \mathcal{X}}(|I_{\vec{y}}(\vec{z})|)| > 1$. Now either $\dim S = n - q$ in which case there exists an ϵ-ball B that is a subset of S around y such that all points in B reveal the same point as $\vec{y}$, or $\dim S < n - q$ in which case the probability of selecting S or any point in it is zero. So, with probability 1, Algorithm 1 finds $n - q + 1$ suitable points that all reveal the same $\vec{x} \in \mathcal{X}$. From this the attacker can determine $|I_{\vec{y}}(\vec{x})|$ for all points $\vec{y} \in R_q$. In particular, the attacker can recover $\{\vec{y} \in R_q : |I_{\vec{y}}(\vec{x})| = 0\}$ which, again by the assumption of d-wise independence, is an $n - (q + 1)$-dimensional affine subspace of R. $\qquad\square$

J Baseline Attack

This section discusses some baseline attacks for reconstructing the target dataset. Each *baseline* attack model generates a static batch of transparency queries, i.e. new queries are not based on the attacker's

past queries. An attacker who has some prior knowledge on the dataset structure can successfully recover significant chunks of the training data; in what follows, we consider three different scenarios.

Uniform samples   With no prior knowledge on data distributions, an attacker samples points uniformly at random from the input space; this attack model is not particularly effective (Figure 14a): even after observing 1,000 queries with 10 training points revealed per transparency query, less than 2% of the Dog/Fish dataset and $\sim 3\%$ of the Hospital dataset are recovered. Moreover, the recovered images are unrepresentative of the data: since randomly sampled images tend to be white noise, the explanation images offered for them are those most resembling noise.

Marginal distributions   In a more powerful attack scenario, the attacker knows features' marginal distributions, but not the actual data distribution. In the case of images, the marginal distributions of individual pixels are rather uninformative; in fact, sampling images based on individual pixel marginals results in essentially random images. That said, under the Inception model, an attacker can sample points according to the marginal distribution of the latent space features: the weights for all nodes (except the last layer) are public knowledge; an attacker could reconstruct images using latent space sampling. Figure 14b shows results for the Hospital dataset, and the Dog/Fish dataset under the inception model. This attack yields far better results than uniform sampling; however, after a small number of queries, the same points tended to be presented as explanations, exhausting the attacker's capacity to reveal additional information.

Actual distribution   This attack model offers access to the actual dataset distribution (we randomly sample points from the dataset that were not used in model training). This reflects scenarios where models make predictions on publicly available data. Using the actual data distribution, we can recover significant portions of the training data (Figure 14c). We again observe a saturation effect: additional queries do not improve the results significantly.
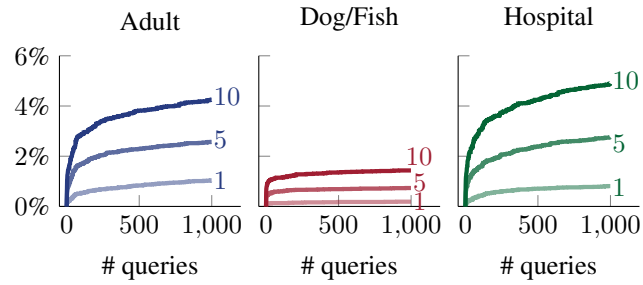
(a) Uniform datapoint sampling.
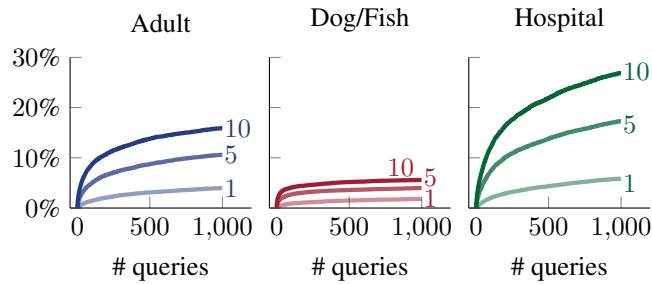
(b) Marginal feature distribution sampling (for the Dog/Fish dataset points are sampled in the latent space).
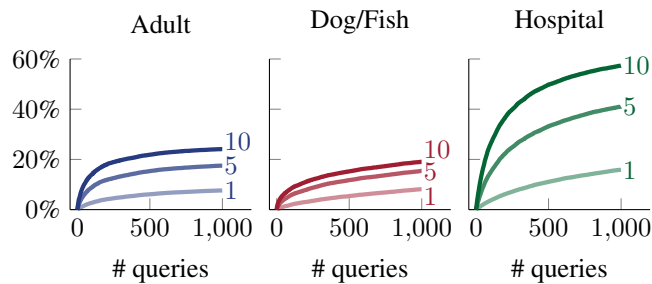
(c) True point distribution sampling.

Figure 14: % of training data revealed by an attacker using different sampling techniques, with $k \in \{1, 5, 10\}$ explanation points revealed per query.